MHD Flow of Cellulose Derivatives and Dilute Suspensions Rheology of Its Nanocrystals

S. E. E. Hamza

Physics Department, Faculty of Science, Benha University, Benha, Egypt

Abstract   The study of cellulose derivatives and magnetic field effects on their rheological properties (magnetorheological) is of evident practical importance because its ability to orient under the action of external fields. The orientation process is of great importance owing to the possibility of changes in structure and final products. The aim of this work was to study theoretically the effects of magnetic field on rheological behavior of some cellulose derivatives solutions. The studied samples are Ethyl cellulose (EC), Hydroxyethyl cellulose (HEC), Hydroxypropyl cellulose (HPC) and Carboxymethyl cellulose (CMC) dissolved in a suitable solvents. The influence of eight different solvents on solutions viscosity was investigated. Vshivkov and his group at the Department of Macromolecular Compounds at the Ural Federal University investigated experimentally the changes in magnetorheological properties of these solutions by using a Rheotest RN 4.1 rheometer. Their works covered the shear rates $0 \leq \dot{\gamma} \leq 15 \text{ s}^{-1}$ and concentration range from 0.04 to $0.41 \text{wt}\%$. In this paper, we reconsider Vshivkov et al. works through collecting their experimental data and carry out its theoretical analysis based on Giesekus model for viscoelastic polymers. This model gives more accurate results and takes into account the effects of viscoelastic shear thinning characteristics, decreasing viscosity with increasing shear rate. The regions of existence of isotropic and anisotropic phases and their concentration dependence were discussed. It is found that a magnetic field increases the viscosities of all solutions under consideration. The study was extended to report the viscosity data of dilute aqueous suspension of cellulose nanocrystals (CNC). It has been treated as a dilute fiber suspension whose concentrations ranging from 0.5 to 8 wt% and its rheology are analyzed using Giesekus model. The orientation of CNC nanoparticles are described in terms of the fiber's second– and fourth–order orientation tensors established by Advani and Tucker. Finally, for adequate prediction of viscoelastic shear thinning characteristics of CNC suspensions as a function of both shear rate and concentration, simple correlations were proposed in terms of an exponential function.

Keywords   MHD, Cellulose derivatives, Dilute Fiber suspension, Cellulose nanocrystals, Giesekus model

1. Introduction

Cellulose is the most abundant polymer on Earth, which makes it the most common organic compound. It is the primary constituent of wood, paper and cotton. Cellulose is linear and rigid polymer consisting of a cyclic structure of anhydroglucose units. When these units are hooked together, the structure of cellulose becomes as shown in Fig. 1a. The chemical character and reactivity of cellulose is determined by the presence of three hydroxyl (OH) groups in the glucose units, one primary and two secondary groups. The hydroxyl groups play an important role in the solubility of cellulose. The relative stiffness and rigidity of the cellulose molecule is mainly due to the intramolecular hydrogen bonding. This property is reflected in its high viscosity in solution,   a high tendency to crystallize, and its ability to

form fibrillar strands. Cellulose chains have a strong tendency to aggregate and to form highly ordered structures and structural entities. The history of the supramolecular structure of cellulose, started as early as 1913 when Nishikawa and Ono discovered the structure of fibrous cellulose by the well–defined X–ray diffraction patterns [1]. This finding lead to the conclusion that individual cellulose molecules tend to arrange themselves in a highly organized manner leading to a crystalline state. Based on these findings, scientists developed the fringed fibrillar model of the structure, which is still accepted theory of the supramolecular structure. As shown in Fig. 1b, the latticework represents the highly ordered (crystalline) region whereas elongated lines represent the low ordered (amorphous) regions. The supramolecular model of cellulose is based on the organization of cellulose chains into a parallel arrangements of crystallites and crystallite strands, which are the basic elements of the CNC fiber [2]. The intermolecular hydrogen bonding are considered to be the major contributors to the structure of cellulose, and is regarded as the predominant factor responsible for uniform

packing [3]. Today experimental evidence describes a two–phase model, which clearly divides the supramolecular structure into two regions: low ordered (amorphous) and highly ordered (crystalline) excluding the medium ordered regions completely [4].

While unmodified cellulose is insoluble in water, modification of the cellulose chain by attachment of small substituents may result in water solubility properties. Published information suggests that, the secondary hydroxyl present in a side chain is available for reaction with the oxide and chaining out may take place. In 1956, Flory [5] predicted that polymers with stiff linear chains would form ordered phases in their respective melt and in concentrated solutions. In 1980, this behaviour was reported for cellulose derivatives, such as HPC in water, which at high concentrations can reflect visible light due to its nematic structure [6]. HPC was also the first cellulosic derivative reported to form spontaneous anisotropic solutions when dissolved in aqueous and organic solvents [7]. Since that discovery, other cellulose derivatives including: ethyl cellulose (EC), HEC, CMC, and cellulose itself have also been reported to form ordered solutions [8-14].

When cellulose is etherified, the hydroxyls (OH) are replaced by the etherifying reagent. The final product is characterized by the degree of substitution (DS) which it is the average number of hydroxyls substituted per unhydroglucose unit. Therefore, EC is a derivative of cellulose in which some of the hydroxyl groups on the repeating glucose units are converted into ethyl ether groups. The properties of EC, as those of other cellulose derivatives, depend primarily up on the degree of substitution. It is practically insoluble in water but is soluble in varying proportions in certain organic solvents [15, 16]. While some solvents are excellent in dissolving EC polymer, they have limited or no application in the pharmaceutical industry because of their unacceptable effect on environment and health. EC find use in many applications, e.g. as water binders, film forming agents and in controlled release [17, 18]. They have been used in the fields of biotechnology, paints and foods [19-21]. Although interest in aqueous dispersions of ECs continues to interest, solvent–based EC extended release coating applications also continue to grow. The pure CMC is white or milk white fibrous powder or particles, odorless and tasteless. It is insoluble in organic solvents such as methanol, alcohol, diethyl ether, acetone, chloroform and benzene but soluble in water. Water solubility of CMC is affected by its DS and viscosity.
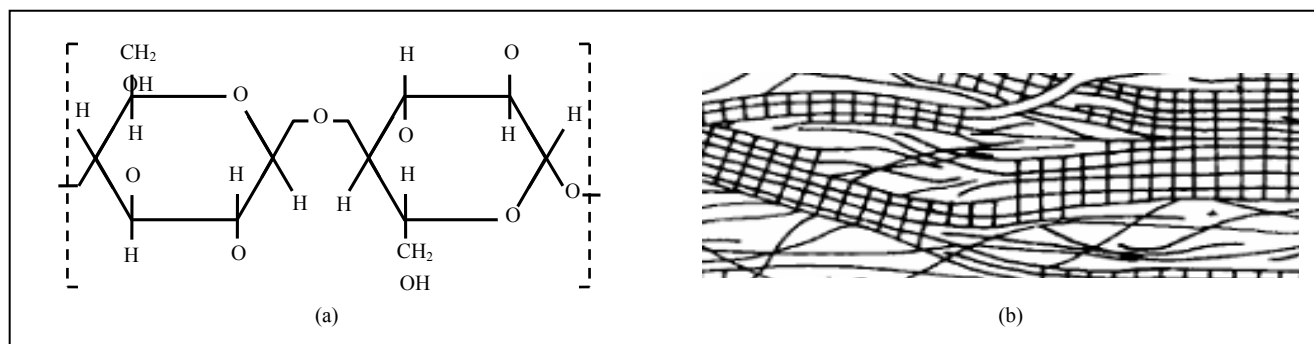

Figure 1.   (a) Structure of cellulose, (b) Fringed fibril model of the supramolecular structure of cellulose

Table 1.   Physical Properties of Used Cellulose Derivatives and Their Suitable Solvents; DMF–Dimethyl Formamide, DMAA– Dimethyl Acetamide, DMAA*– Dimethyl Acetamide with Macromolecules, DMSO– Dimethyl Sulfoxide

Cellulose derivative	Suitable solvents	(DS)	Molecular weight		
			M_w	M_η	M_n
Ethyl cellulose (EC)	DMF DMAA DMAA*	1.5, 2.5, 2.6	1.6×10^5	2.6×10^4	---
Hydroxyethyl cellulose (HEC)	Water DMF DMF*	2.5	---	6.2×10^4	6.2×10^4
Hydroxypropyl cellulose (HPC)	Water Ethanol Ethylene glycol DMSO	2.25, 3.2, 3.6	1.6×10^5 1.0×10^5	---	1.6×10^5
Carboxymethyl cellulose (CMC)	Water	0.7	---	1.2×10^5	---

Cellulose insolubility nature in common organic solvents and in water is due to the fact that the hydroxyl groups are responsible for the extensive hydrogen bonding network. In order to dissolve cellulose, one has to find a suitable solvent to break down the hydrogen bond network, i.e. the initial supramolecular structure of cellulose should be destroyed in order to obtain a homogeneous (one–phase) solution. The suitable solvents and their physical properties used in this study are listed in Table 1. The molecular weights of polymers are much larger than the small molecules usually encountered in organic chemistry. Most chain reaction produce chains with many different lengths, so polymers also differ from small molecules in that the polymer molecular weights are average values. One of the oldest methods of measuring the average molecular weight of polymers is by solution viscosity. The viscosity–average molecular weight lies somewhere between the number average and the weight average. Therefore, the molecular weights that are important in determining polymer properties are the number–average, M_n, the weight–average, M_w, and the viscosity–average, M_η molecular weights.

Polymer molecules are long chain molecules composed of many repeating units. The bonds along the polymer backbone are continually rotating, and as a result, the molecule itself is continually changing its orientation and configuration. Polymer solutions can be considered as liquid mixtures made of long macromolecular chains, and small molecules of solvent [22]. At rest, the chains of polymers are randomly entangled and they do not set up the polymer structure. When the fluid is in motion, the chains tend to align themselves parallel to the direction of flow. This tendency increases with increasing in shear rate, so that the effective viscosity decreases [23]. In dilute polymer solutions, the rheology of solution is depends solely on the dynamics of an individual chain and the number of chains (i.e. concentration) in the system. At high concentrations, interactions between polymer molecules impact the rheology in a significant way. As concentration increases, polymer solutions exhibit a change from fluid–like to more elastic–like behavior [24]. Viscosities of solutions of polymeric liquids are known to be variable quantities which decreases with increasing shear rate. This shear–thinning effect has been known for a long time, but its adequate explanation is still absent. In the case of concentrated solutions, a varying viscosity is assumed to be due to the entanglement of macromolecular chains. For a dilute solution viscosity variations are associated with a behavior of separate molecules in the flow, i.e., their deformation, orientation, etc.

In both cases indicated above, attraction forces between macromolecules are neglected. An alternative explanation of shear thinning is based on an assumption of macromolecular cross–linking. Cross–links are considered to be weak; they disappear and reappear again as a result of thermal motion. An average number of cross–links in the shear flow decreases when the shear rate is increased, which leads to a decreased apparent viscosity.

The orientation of macromolecules in polymer solutions under the influence of an external magnetic field is of great importance owing to the possibility of changes in structure and the products formation. The molecules of cellulose and its derivatives have a rigid spiral conformation and can undergo ordering. Under the effect of magnetic field these macromolecules may be rearrange themselves so that taking the same direction as the magnetic field lines (i.e. oriented parallel with the magnetic lines), a circumstance that lead to an increase in polymer viscosity. The effects of shear rate, magnetic field and concentration on the rheological properties of cellulose derivatives were described by Vshivkov alone [25] and with his collaboration [26-30].

In recent years, cellulose nanocrystals (CNC) has been used in a wide variety of applications because of their nano–sized dimensions and other important properties. An increasing number of studies in the area o f cellulose nano composites have also been reported during the last few years because of the enormous interest in their industrial applications. The rheology of suspensions provide critical information for products in many industrial applications. The addition of nanoparticles to polymers greatly changed the rheological properties of their suspension. In order of suspension to give proper product performance, they must be stable. The stability of the final product is very complex process because of the variation in size and shape of nanoparticles. CNC are rod–like particles product from natural cellulose materials through mechanical disintegration [31-33]. In this process CNCs are conventionally rod–shaped nano–scale entities 5–20 nm in diameter and hundreds or thousands of nm in length. The flow properties of suspensions prepared from cellulose derivatives have been previously studied and its behaviour under shear has also been characterized [34-36].

The determination of rheological properties of dilute suspensions of cellulose nanocrystals systems are very important for its characterization. Various studies have shown that the viscoelastic properties of nano–composites depend strongly on the CNC content. In fact, the viscosity of all CNC–polymer nano–composites increased with increasing CNC content. Bercea and Navard [37] studied the viscosity of aqueous suspensions of tunicate cellulose nanocrystals and found that the phase state of CNC suspension can be determined based on changes in viscosity. Urena–Benavides et al. [38] investigated the rheological behaviour of cotton CNC suspension, and found that the phase behavior of CNC suspensions can be divided into four regions with different scaling relationships between rheological parameters and CNC concentrations. Lu et al. [39] studied the rheological and phase behaviors of rod–like nanocrystalline cellulose suspensions in aqueous media. They fitted the relative viscosity of the CNC suspension in the full concentration range tested. The fitting curves show that the viscosity increases monotonically with CNC concentration. Shafiei et al. [40] studied the effects of concentration and temperature on the rheological properties of micro–fibrillar cellulose aqueous suspensions.

In this paper, we reconsider Vshivkov et al. [26-30] experimental data for cellulose derivatives, Lu et al. [39] and Shafiei et al. [40] data for dilute aqueous suspensions of CNC. We collect and reorder their experimental data and carry out its theoretical analysis based on Giesekus model for viscoelastic polymers. As we have seen from our previous papers [41, 42], this model takes into account the effects of shear thinning characteristics on the viscosity of the polymer solutions and gives more accurate results. Also, the effects of magnetic field on the magnetorheological properties of cellulose derivatives solutions are investigated. The chosen model fits adequately the experimental data of Vshivkov et al. for cellulose derivatives. Since CNCs are rod–like nanoparticles in suspension, so it has been treated as a dilute fiber suspension. The collected data were described by using the equation established by Advani and Tucker [43] which gives more accurate results.

2. Problem Formulation

2.1. Governing Equations for Cellulose Derivatives

In the present paper, circular Couette flow occurs in the gap between two rotating concentric cylinders rheometer is investigated. The inner cylinder of radius R_1 rotates with constant angular velocity Ω. The apparatus has a height L which is much larger than the radius of either cylinder, see Fig. 2. In general, the momentum and continuity equations of steady MHD flow of incompressible viscoelastic fluid are given by:

$$\rho \underline{v} \cdot \nabla \underline{v} = -\nabla P + \nabla \cdot \underline{\underline{\tau}} + \rho \underline{b}, \qquad (1)$$

$$\nabla \cdot \underline{V} = 0, \qquad (2)$$

where ρ, $\underline{v}$, P, $\underline{\underline{\tau}}$, and "$\underline{b}$" are respectively the density, velocity, pressure, extra stress tensor and the body force per unit mass. Notice that, in the presence of an applied magnetic field, the term $\rho \underline{b} = \underline{F}_B = \underline{J} \times \underline{B}$ represents the Lorentz force due to magnetic field where $\underline{J}$ is the current density and $\underline{B}$ is the magnetic induction vector.

Many flow models have been proposed, which are useful for treatment of experimental data or for describing flow behavior. Such mathematical models range from the very simple to the very complex models. In this paper we select Giesekus model to describe the stress tensor for the polymers under consideration. The extra stress tensor $\underline{\underline{\tau}}$ for this model can be written as [44-46]:

$$\underline{\underline{\tau}} = \underline{\underline{\tau}}_s + \underline{\underline{\tau}}_p, \qquad (3)$$

$$\underline{\underline{\tau}}_s = 2\eta_s \underline{\underline{\dot{\gamma}}}, \qquad (4)$$

$$\underline{\underline{\tau}}_p + \lambda_1 \overset{\nabla}{\underline{\underline{\tau}}}_p + \alpha \frac{\lambda_1}{\eta_p}\left(\underline{\underline{\tau}}_p \cdot \underline{\underline{\tau}}_p\right) = 2\eta_p \underline{\underline{\dot{\gamma}}}. \qquad (5)$$

Here $\underline{\underline{\tau}}$ is decomposed into a polymer contribution $\underline{\underline{\tau}}_p$

and a Newtonian solvent contribution $\underline{\underline{\tau}}_s$. Also $\underline{\underline{\dot{\gamma}}} = \frac{1}{2}[\nabla \underline{v} + (\nabla \underline{v})^T]$ denotes the shear tensor and the superscript ∇ stands for the upper–convected derivative. The parameters η_s and η_p are the solvent and polymer contributions to the zero–shear–rate viscosity, λ_1 is relaxation time and α denotes Giesekus mobility factor ($0 \le \alpha \le 1$). It is convenient to rewrite Eqs. (3) to (5) as a single constitutive equation by replacing $\underline{\underline{\tau}}_p$ in the last equation with $\underline{\underline{\tau}} - \underline{\underline{\tau}}_s = \underline{\underline{\tau}} - 2\eta_s \underline{\underline{\dot{\gamma}}}$. This leads to:

$$\underline{\underline{\tau}} + \lambda_1 \overset{\nabla}{\underline{\underline{\tau}}} + a\frac{\lambda_1}{\eta_o}\left(\underline{\underline{\tau}} \cdot \underline{\underline{\tau}}\right) - 2a\lambda_2\left(\underline{\underline{\tau}} \cdot \underline{\underline{\dot{\gamma}}} + \underline{\underline{\dot{\gamma}}} \cdot \underline{\underline{\tau}}\right) =$$
$$2\eta_o\left[\underline{\underline{\dot{\gamma}}} + \lambda_2 \overset{\nabla}{\underline{\underline{\dot{\gamma}}}} - 2a\frac{\lambda_2^2}{\lambda_1}\left(\underline{\underline{\dot{\gamma}}} \cdot \underline{\underline{\dot{\gamma}}}\right)\right], \qquad (6)$$

where η_o is the zero shear rate viscosity, λ_2 is the retardation time and "a" is the modified mobility parameter. These parameters are related through the relations:

$$\eta_o = \eta_s + \eta_p; \quad \lambda_2 = \lambda_1\frac{\eta_s}{\eta_o}; \quad a = \frac{\alpha}{1-(\lambda_2/\lambda_1)}. \qquad (7)$$

Giesekus model is a special case of the Oldroyd 8–constant model to which a term involving $\underline{\underline{\tau}} \cdot \underline{\underline{\tau}}$ is added .The inclusion of $\underline{\underline{\tau}} \cdot \underline{\underline{\tau}}$ term in Eq. (6) gives material functions that are more realistic than any other model. For example, large decreases in the viscosity and normal stress coefficients with increasing shear rate are possible.

In the present study, a cylindrical coordinate system (r, θ, z) is used. The magnetic field is applied either in x– or in z–direction as shown in Fig. 2 such that $\underline{B} = B_x\hat{i} + B_z\hat{k}$. From the physics of this problem, the flow is assumed to be axisymmetric ($\partial/\partial\theta = 0$). Therefore, the velocity field, magnetic field vector and the stress tensor can be written as:

$$\underline{v} = [0, \ v_\theta(r), \ 0], \qquad (8a)$$

$$\underline{B} = [B_x\cos\theta, \ 0, \ B_z], \qquad (8b)$$

$$\underline{\underline{\tau}} = \begin{bmatrix} \tau_{rr} & \tau_{r\theta} & \tau_{rz} \\ \tau_{\theta r} & \tau_{\theta\theta} & \tau_{\theta z} \\ \tau_{zr} & \tau_{z\theta} & \tau_{zz} \end{bmatrix}, \qquad (8c)$$

with the choice of the velocity given in Eq. (8a), the continuity equation is satisfied automatically and Lorentz force takes the form:

$$\underline{F}_B = -\sigma\left(B_r^2 + B_z^2\right)\underline{v}, \qquad (9)$$

where σ is the electrical conductivity of the fluid, $B_r (= B_x\cos\theta)$ and B_z are the strength of an imposed uniform magnetic field in r–and z–directions respectively. With these simplifications, the momentum equation reduces to:

$$\rho \frac{v_\theta^2}{r} = \frac{dP}{dr}, \qquad (10)$$

$$\frac{d\tau_{r\theta}}{dr} + \frac{\tau_{r\theta} - \tau_{\theta r}}{r} + \sigma\left(B_r^2 + B_z^2\right)v_\theta = 0. \qquad (11)$$

The boundary conditions are such that the inner cylinder rotates with constant angular velocity $\underline{\Omega} = \Omega\hat{z}$. The velocity at outer cylinder vanishes, $\underline{v}(R_2) = 0$, while at the surface of the inner cylinder is:

$$\underline{v}(R_1) = (\Omega R_1)\hat{\theta}. \qquad (12)$$

The nonlinear stress term $\underline{\underline{\tau}} \cdot \underline{\underline{\tau}}$ in Eq. (6) make it more difficult to obtain analytical solutions for the mathematical functions.

2.2. Viscosity and Elastic Characteristics

Experimental analysis of shear rate dependent viscosity for cellulose derivatives solutions and dilute suspensions of CNC requires high accuracy measurements, because viscosities of these materials only slightly exceed those of the solvents. This is one of the reasons why viscometric studies are essentially absent for dilute polymer solutions. Something of the shear dependent viscosity of dilute polymer solutions can be gained from experiments [47]. An important problem in this field is the establishment of rheological characteristics that determine hydrodynamic behavior of polymeric solutions, and development of techniques for measuring these characteristics. Maxwell's and Jeffrey's models of viscoelastic fluids are very simple and unable for the behavior description of the dilute polymer solutions.

Giesekus model is characterizes by four parameters η_o, λ_1, λ_2 and a, which can be treated as the model's parameters. Limiting cases of the Giesekus model include the Newtonian fluid ($\alpha = \lambda_1 = \lambda_2 = 0$), the upper-convected Maxwell fluid ($\alpha = \lambda_2 = 0$) and the Oldroyd-B fluid ($\alpha = 0$). However, by adding a small retardation term (e.g., $\lambda_2/\lambda_1 = 10^{-3}$), the magnitude of the shear stress is always increasing with increasing shear rate. In general we must require $0 < \alpha < 1$ for realistic shear thinning and $\alpha > 1$ for shear thickening fluids and in general $\lambda_1 > \lambda_2$. Giesekus model yields the following material functions (apparent viscosity η, first and the second normal stresses Ψ_1 and Ψ_2); [46]:

$$\eta(\dot{\gamma}) = \eta_o\left\{\frac{\lambda_2}{\lambda_1} + \left(1 - \frac{\lambda_2}{\lambda_1}\right)\frac{(1-f)^2}{1+(1-2\alpha)f}\right\}, \qquad (13)$$

$$\Psi_1(\dot{\gamma}) = 2\eta_o(\lambda_1 - \lambda_2)\left\{\frac{f(1-\alpha f)}{(\lambda_1\dot{\gamma})^2\alpha(1-f)}\right\}, \qquad (14)$$

$$\Psi_2(\dot{\gamma}) = \eta_o(\lambda_1 - \lambda_2)\left\{\frac{-f}{(\lambda_1\dot{\gamma})}\right\}, \qquad (15)$$

where

$$f = \frac{1-\chi}{1+(1-2\alpha)\chi}, \qquad (16)$$

and

$$\chi^2 = \frac{\sqrt{1+16\alpha(1-\alpha)(\lambda_1\dot{\gamma})^2}-1}{8\alpha(1-\alpha)(\lambda_1\dot{\gamma})^2}. \qquad (17)$$
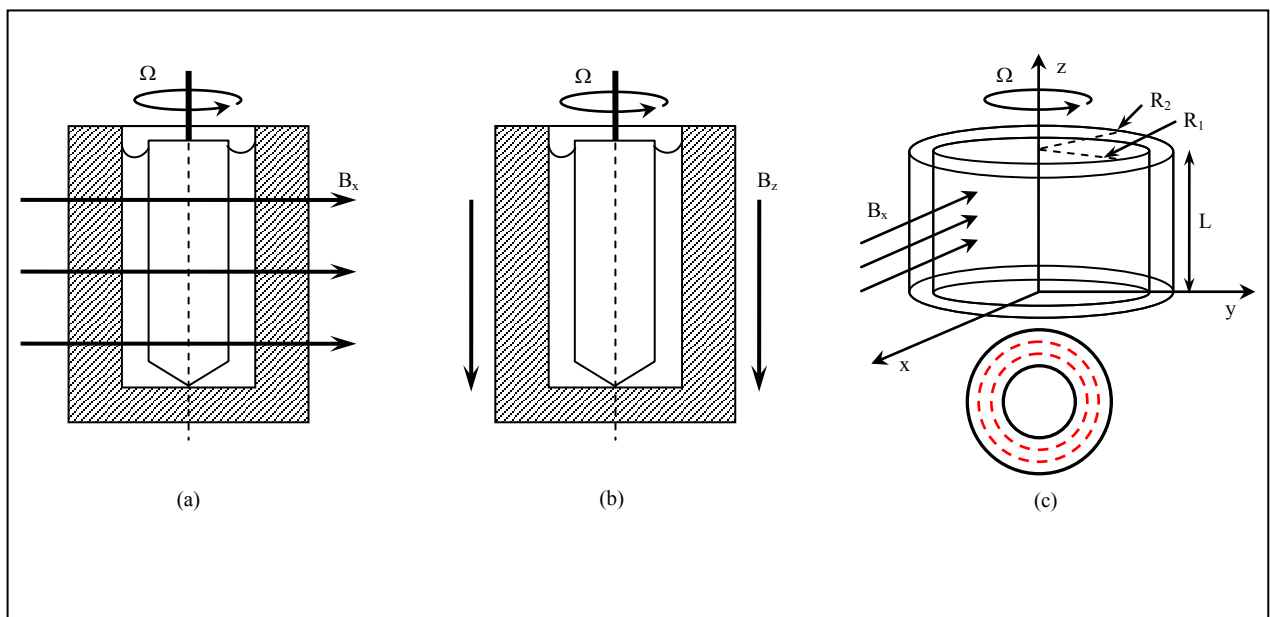

Figure 2. Schematic representation of viscosity determination with magnetic lines of force directed (a, c) perpendicular and (b) parallel to the rotational axis of the rotor

Ψ_1 and Ψ_2 are not taken into account here because of they can be measured only in un–symmetric regions such as eccentric cylinders or cone and plate rheometers. From this survey one can expect that sufficient realistic results will be observed for dilute solutions. It can thus be assumed that Giesekus model can be used in determination all rheological properties of cellulose derivatives and dilute CNC suspensions.

3. Governing Equations

3.1. CNC Suspension as a Fiber

The rheological properties are the results of interaction among CNC fibers in the suspension flow. The volume fraction V_f (total volume of CNC fiber in a unit volume of suspension) and aspect ratio a_r (ratio of CNC fiber length to diameter) are two parameters influencing the rheological properties of suspensions. CNC Fiber interactions depend on its concentration, $V_f a_r^2$, and length. Hence, suspensions are classified according to its concentration as [48, 49]:

$$\left.\begin{array}{c} \text{dilute} \\ \text{semi–dilute} \\ \text{concentrated} \end{array}\right\} \text{ if } \left\{\begin{array}{l} V_f a_r^2 < 1, \\ 1 < V_f a_r^2 < a_r, \\ V_f a_r^2 > a_r. \end{array}\right. \quad (18)$$

The rheological properties of CNC fiber suspensions are classified as the following:

- Dilute, low CNC fiber concentration is one in which the CNC fibers are never close to one another and do not interact [50, 51]. Therefore, each CNC fiber can freely rotate without any hindrance from surrounding CNC fibers with three rotational degrees of freedom.
- Semi–dilute, intermediate CNC fiber concentration suspension would have no mechanical contact between the CNC fibers, but the hydrodynamic interactions become significant.
- Concentrated suspensions, in which the CNC fiber orientation behavior becomes very complex. The average distance between two neighboring CNC fibers is less than its diameter. Therefore, CNC fiber cannot rotate independently, except about its own symmetrical axis. Any motion of the CNC fibers must involve a cooperative effort of all surrounding CNC fibers and fiber–fiber contacts are dominate.

3.2. CNC Fiber Orientation Description

The properties of CNC fiber suspension are highly dependent on the orientation of the CNC fibers in its flow domain. The orientation of a single CNC fiber within a continuous medium matrix can be described in spherical coordinate system by the unit vector $\underline{p}(\theta, \varphi)$ aligned along the axis of the CNC fiber as shown in Fig. 3, where $\underline{p}$ is parallel to the major axis of CNC fiber with components:

$$p_1 = \sin\theta\,\cos\varphi\,; \ p_2 = \sin\theta\,\sin\varphi\,; \ p_3 = \cos\theta, \quad (19)$$
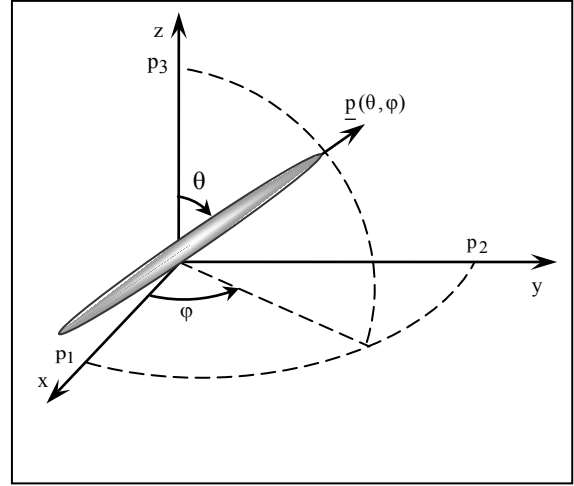
with, $p_1^2 + p_2^2 + p_3^2 = 1$.

Figure 3.   Orientation of a single CNC fiber

Let us now introduce the probability density function $\Psi(\theta, \varphi)$ whose value gives the probability of CNC fiber oriented between the angles θ_i and $\theta_i + d\theta$ and φ_i and $\varphi_i + d\varphi$ as:

$$p(\theta_i \le \theta \le \theta_i + d\theta, \ \varphi_i \le \varphi \le \varphi_i + d\varphi) = \\ \Psi(\theta, \varphi)\sin\theta\,d\theta\,d\varphi, \quad (20)$$

with the normalization condition on the unit sphere,

$$\int_0^{2\pi} \int_0^{\pi} \Psi(\theta, \varphi)\sin\theta\,d\theta\,d\varphi = 1. \quad (21)$$

The distribution function $\Psi(\theta, \varphi)$ is a complete description if the orientation of a single CNC fiber is unrelated to any other neighboring fibers. However, the calculations with the distribution function are too computationally cost when applied to industrially relevant flows. Therefore, the introducing of orientation tensors is a suitable way for describing the orientation state of CNC fibers. The orientation tensors are defined as [43, 52],

$$S_{ij} = \oint_{\Re^2} p_i p_j \Psi(\underline{p})\,d\Re, \quad (22)$$

where $\Re^2$ is the unit sphere. The second–order tensor S_{ij} consists of nine components, however, due to symmetry ($S_{ij} = S_{ji}$) the components is reduced to six. These tensor components can be written as:

$$S_{ij} = \begin{bmatrix} \sin^2\theta\cos^2\varphi & \sin^2\theta\sin\varphi\cos\varphi & \sin\theta\cos\theta\cos\varphi \\ \bullet & \sin^2\theta\sin^2\varphi & \sin\theta\cos\theta\sin\varphi \\ \bullet & \bullet & \cos^2\theta \end{bmatrix}, \quad (23)$$

the components of the fourth–order tensor S_{ijkl} have all information needed to describe the CNC fiber orientation.

The normalization condition in Eqs (21) show the two fundamental symmetry properties of S_{ij}:

$$S_{ij} = S_{ji} \text{ and } S_{ii} = 1. \qquad (24)$$

The tensors have a simple physical interpretation. If the CNC fibers are randomly distributed, the second–order tensors are said to be:

$$S_{ij} = \frac{1}{3}\delta_{ij}, \qquad (25)$$

or

$$S_{ij} = \begin{bmatrix} \frac{1}{3} & 0 & 0 \\ 0 & \frac{1}{3} & 0 \\ 0 & 0 & \frac{1}{3} \end{bmatrix}. \qquad (26)$$

Figure 4a shows isotropic orientation state, with equal orientation distribution in all directions. If all the CNC fiber lie in the xy–plane, Fig. 4b, which corresponds to planer random orientation state S_{ij} is simply:

$$S_{ij} = \begin{bmatrix} \frac{1}{2} & 0 & 0 \\ 0 & \frac{1}{2} & 0 \\ 0 & 0 & 0 \end{bmatrix}. \qquad (27)$$

For perfectly aligned orientation in x–direction, Fig. 4c, S_{ij} is written as:

$$S_{ij} = \begin{bmatrix} 1 & 0 & 0 \\ 0 & 0 & 0 \\ 0 & 0 & 0 \end{bmatrix}. \qquad (28)$$
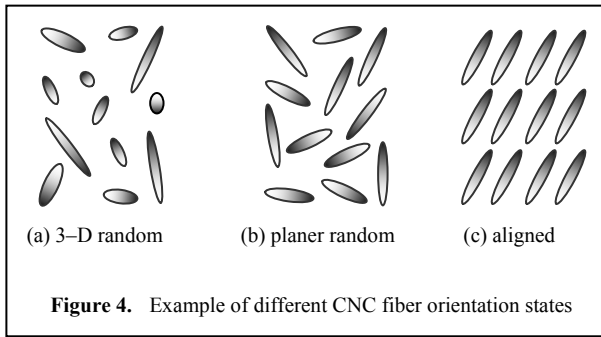

Figure 4. Example of different CNC fiber orientation states

(a) 3–D random   (b) planer random   (c) aligned

It is well understood that CNC fibers orient in response to flow kinematics, while the suspension rheology is defined in the concentration and orientation of the suspended fiber. The motion of a single CNC fiber in a Newtonian flow can be described by Jeffery's model in its vector form as:

$$\frac{D\underline{p}}{Dt} = -\underline{\underline{\omega}} \cdot \underline{p} + \beta\left(\underline{\underline{\dot{\gamma}}} \cdot \underline{p} - \underline{\dot{\gamma}} : \underline{ppp}\right), \qquad (29)$$

where β is a constant defining as the shape factor of the fiber, it depends on the fiber aspect ratio a_r as:

$$\beta = \frac{a_r^2 - 1}{a_r^2 + 1}, \qquad (30)$$

for slender CNC fiber $\beta \to 1$. In Eqs. (29), $D/Dt = \partial/\partial t + (\underline{v} \cdot \nabla)$ is the material time derivative, $\underline{\underline{\dot{\gamma}}} = \frac{1}{2}\left[\nabla \underline{v} + (\nabla \underline{v})^T\right]$ is the shear rate or deformation tensor and $\underline{\underline{\omega}} = \frac{1}{2}\left[\nabla \underline{v} - (\nabla \underline{v})^T\right]$ is the vorticity tensor. Instead of performing the integration and tedious calculation of the distribution function, an equivalent system of differential equations can be written that characterizes the orientation evaluation in terms of the tensors $\underline{\underline{S}}_2$ as:

$$\frac{D\underline{\underline{S}}_2}{Dt} = -\left(\underline{\underline{\omega}} \cdot \underline{\underline{S}}_2 - \underline{\underline{S}}_2 \cdot \underline{\underline{\omega}}\right) + \beta\left(\underline{\underline{\dot{\gamma}}} \cdot \underline{\underline{S}}_2 + \underline{\underline{S}}_2 \cdot \underline{\underline{\dot{\gamma}}} - 2\underline{\underline{\dot{\gamma}}} : \underline{\underline{S}}_4\right). \quad (31)$$

The evolution equation of any orientation tensor contains next higher even–order tensor; say $\underline{\underline{S}}_2$ in Eq. (31) contains $\underline{\underline{S}}_4$. Thus, one needs a closure approximation to close the set of the evolution equations of the orientation tensors. A fourth–order closure may be expressed as:

$$\underline{\underline{S}}_4 \approx F(\underline{\underline{S}}_2), \qquad (32)$$

where "F" is a function of the second–order tensor $\underline{\underline{S}}_2$. There are many methods proposed to address the closure problem. Most types of closure approximations is the linear one which originally introduced by Hand [53]:

$$S_{ijkl} = \frac{-1}{(4 + N_L)(2 + N_L)}\left(\delta_{ij}\delta_{kl} + \delta_{ik}\delta_{jl} + \delta_{il}\delta_{jk}\right) + \\ \frac{1}{(4 + N_L)}\left(S_{ij}\delta_{kl} + S_{ik}\delta_{jl} + S_{il}\delta_{jk} + S_{kl}\delta_{ij} + S_{jl}\delta_{ik} + S_{jk}\delta_{il}\right), \qquad (33)$$

where δ_{ij} is the unit tensor and N_L refers to a space dimensions; i.e.,

$$N_L = \begin{cases} 2 & \text{in } 2D, \\ 3 & \text{in } 3D. \end{cases} \qquad (34)$$

This closure approximation is exact for a random distribution of CNC fiber orientations (an isotropic suspension). Also, it is exact for a completely isotropic distribution of CNC fiber orientations,

$$S_{ijkl} = S_{ij}S_{kl}, \qquad (35)$$

which is exact for aligned CNC fiber.

3.3. Constitutive Equation for CNC Fiber Suspensions

Several constitutive models have been proposed to describe the stress tensor for a suspension of CNC fibers in a Newtonian fluid. In general, the total extra stress tensor for the suspension, $\underline{\underline{\tau}}$, is taken to be the sum of the stress contributions from the Newtonian solvent fluid $\underline{\underline{\tau}}_s$, and from the fiber, $\underline{\underline{\tau}}_f$. Hence, the resulting constitutive equations for the suspension can be expressed as [54]:

$$\underline{\underline{\tau}} = \underline{\underline{\tau}}_s + \underline{\underline{\tau}}_f, \qquad (36)$$

$$\underline{\underline{\tau}}_s = -P\underline{\underline{I}} + \eta_s \underline{\underline{\dot{\gamma}}}, \qquad (37)$$

To model the fiber stress tensor, Advani and Tucker [43] assumed that:

$$\underline{\underline{\tau}}_f = \eta_s V_f \left[\mu_1 \underline{\underline{\dot{\gamma}}} : \underline{\underline{S}}_4 + \mu_2 \left(\underline{\underline{\dot{\gamma}}} : \underline{\underline{S}}_2 + \underline{\underline{S}}_2 : \underline{\underline{\dot{\gamma}}} \right) + \mu_3 \underline{\underline{\dot{\gamma}}} \right], \quad (38)$$

where μ_i ($i = 1, 2, 3$) are positive material parameters specified by the particle aspect ratio, a_r. For a slender shape, particle thickness can be ignored producing μ_2 and μ_3 equal to zero. Therefore, typical CNC fiber stress tensor for dilute CNC suspensions can be expressed as:

$$\underline{\underline{\tau}}_f = \eta_s \mu_1 V_f \underline{\underline{\dot{\gamma}}} : \underline{\underline{S}}_4, \qquad (39)$$

and

$$\mu_1 = \frac{a_r^2}{\left(\ln 2a_r - \frac{3}{2} \right)} \approx \frac{a_r^2}{\ln a_r}, \qquad (40)$$

3.4. Governing Equations for CNC Suspensions

The total system of the CNC suspensions are governed by the following steady state equations:

- The equation of conservation of linear momentum; Cauchy's dynamical equation of motion,

$$\rho \underline{v} \cdot \nabla \underline{v} = -\nabla P + \nabla \cdot \underline{\underline{\tau}} + \rho \underline{b}, \qquad (41)$$

- Continuity equation (for incompressible fluid);

$$\nabla \cdot \underline{v} = 0, \qquad (42)$$

- CNC Fiber equation of state;

$$\frac{D\underline{\underline{S}}_2}{Dt} = -\left(\underline{\underline{\omega}} \cdot \underline{\underline{S}}_2 - \underline{\underline{S}}_2 \cdot \underline{\underline{\omega}} \right) + \beta \left(\underline{\underline{\dot{\gamma}}} \cdot \underline{\underline{S}}_2 + \underline{\underline{S}}_2 \cdot \underline{\underline{\dot{\gamma}}} - 2\underline{\underline{\dot{\gamma}}} : \underline{\underline{S}}_4 \right). \quad (43)$$

4. Test Materials

From the end of the 2008s, systematic research onto magnetorheological of cellulose derivatives have been performed at the Department of Macromolecular Compounds at the Ural Federal University. The effects of shear rate, magnetic field and concentration on the rheological properties of cellulose derivatives were described by Vshivkov et al. [26-30]. The studied samples of cellulose derivatives are: EC, HEC, HPC and CMC. The used solvents were DMAA, DMAA* (DMAA with macromolecules), DMF, DMSO, ethylene glycol and ethanol.

The corresponding author, molecular weight M_w, DS and the used solvents for each cellulose derivatives are listed in Table 2. The solvent purity was studied through refractive index measurements [26]. The authors were prepared polymer solutions in sealed ampoules at certain temperature and concentration for several weeks.

The CNC particle sample was prepared by acid hydrolysis of commercial dissolved kraft softwood pulp. Pulp was hydrolyzed with 64% sulfuric acid using a 1:8 weight ratio at 50°C for 40min and then diluted with deionized water to quench the reaction. The suspension was then centrifuged at 6000rpm for 10 min neutralized with Na_2CO_3 and dialyzed to remove the salts. Finally, the suspension was dispersed in an ultrasonic bath to achieve a 1-2 wt% concentration stable suspension. CNC particles were obtained in powder form by lyophilizing the suspension. The aqueous nanoparticles suspensions at different fiber concentrations (5.3, 6, 6.6, 7.3, 8 wt% [39] and 0.5, 1, 1.5, 2 wt% [40]) were then prepared and characterized in this study.

Table 2. Summary of Cellulose Derivatives with Its Suitable Solvents and Their Corresponding Author

Materials	solvents	T (K)	C wt %	(DS)	M_w	Author(s)
EC	DMAA	350	0.25	2.5	1.6×10^5	Vshivkov et al. [26]
	DMAA*	370	0.30	1.5		Vshivkov et al. [28]
	DMF	353	0.25	2.6		Vshivkov and Soliman [29]
HEC	DMF	350	0.15	2.5	---	Vshivkov et al. [26]
	DMF*	370	0.15			Vshivkov et al. [28]
	Water	298	0.10			Vshivkov et al. [26]
HPC	Water	298	0.10	2.25	1.6×10^5	Vshivkov et al. [26]
	Ethylene glycol	363	0.15	3.6		Vshivkov and Soliman [29]
	DMSO	368	0.10	3.2	1.0×10^5	Vshivkov and Soliman [30]
	Ethanol	333	0.41			Vshivkov and Soliman [30]
CMC	Water	293	0.04	0.7		Vshivkov and Byzov [27]
CNC	Water	298	5.3, 6, 6.6, 7.3, 8.0	---	---	Lu et al. [39]
			0.5, 1.0, 1.5, 2.0	---	---	Shafiei et al. [40]

5. Viscosity Measurements

Vshivkov and his groups investigated experimentally the changes in magnetorheological properties of cellulose derivatives solutions by using a Rheotest RN 4.1 rheometer over shear rates $0 \leq \dot{\gamma} \leq 15\,\mathrm{s}^{-1}$. Their works covered the concentration range from 0.04 to 0.41wt%. Figure 5 shows schematic representation of Rheotest RN 4.1 rheometer and its installation method in magnetic field. The device is modified by Vshivkov and Soliman [29] utilizes a concentric cylinders geometry in which the inner cylinder of radius R_1 is rotated with angular velocity Ω and the outer cylinder of radius R_2 is held in a fixed position. The shear rate $\dot{\gamma}$ and the dynamical viscosity $\eta(\dot{\gamma})$ of a sample is calculated according to the following equations:

$$\dot{\gamma} = \frac{R_1 \Omega}{R_2 - R_1}, \tag{44}$$

$$\eta(\dot{\gamma}) = \frac{G(R_2 - R_1)}{2\pi R_1^3 L \Omega}, \tag{45}$$

where L is the height of the cylinders and G is the torque on inner cylinder. The assumptions used in deriving Eq. (45) does not hold near the bottom of the viscometer. In order to compensate for this end effect, the bottom of the inner cylinder is actually constructed with a conical shape, as in Figs. 5a and 5c; the flow at the bottom is thus a cone and plate flow. The gap is assumed to be narrow, that is $(R_2 - R_1)/R_1 << 1$. Therefore, the viscosity expression $\eta(\dot{\gamma})$ for this geometry must be corrected to the following form [46]:

$$\eta(\dot{\gamma}) = \frac{G(R_2 - R_1)}{2\pi R_1^3 L \left[1 + (R_1 / 3L)\right]\Omega}. \tag{46}$$

Type of viscometer makes it possible to measure viscosity of aqueous solutions at shear rates from 50 to 200 s^{-1}. High accuracy enabled us to investigate viscosity variations for low concentration solutions, in particular, when the solution viscosity exceeded that of the solvent one.

Solutions viscosity were determined on a modified Rheotest RN 4.1 rheometer with a cylindrical working unit made from a weakly magnetic material, such as brass. A metallic rotor rotating in a magnetic field represents a generator closed on itself. During operations of the generator, a slowdown torque is induced as a result of electromagnetic moment. Therefore, during shear stress measurements, the measured stress exceeds the true stress by a value related to the electromagnetic moment. The true shear stress for solutions was calculated as the difference between the measured and correction values for the same shear rate. The effect of a magnetic field on the rheological properties of solutions was studied with the use of the following two magnets:

- the first magnet, which induces a magnetic field with an intensity of $B_x = 3.7\,\mathrm{kOe}$ and field lines directed perpendicularly to the rotational axis of a rotor.
- the second magnet, with an intensity of $B_z = 3.6\,\mathrm{kOe}$ and field lines parallel to the axis of rotor rotation.

The working unit with a solution was placed into the magnetic field at $298\,\mathrm{K}$ and kept for 20min, then the viscosity in the presence of the magnetic field were measured at an increasing shear rate from 0 to $15\,\mathrm{s}^{-1}$. During magnetic field application, the solution viscosity grows as a result of orientation of chains molecules under a magnetic field in parallel with the line of force. The magnetic field components are $B_r = B_x \cos\theta$ and B_z imposed in r–and z–directions respectively. The, processes occurring during the flow of solutions in the presence of a magnetic field may be represented with the help of Fig. 5 as the following:

- In quadrant I, field lines are parallel to the rotational axis, Fig. 5b. The orientation of molecules chains and the flow direction coincide with opposite directions. In this case, the viscosity may decrease
  $(B_r = B_x \cos 180^o = -B_x)$.
- In quadrant III, field lines are parallel to the rotation axis. The orientation of molecules chains and the flow direction are coincides and are in same directions. In this case, the viscosity may increase
  $(B_r = B_x \cos 0^o = B_x)$.
- In quadrant II, molecules chains are oriented perpendicularly to the flow direction
  $(B_r = B_x \cos 90^o = 0)$. Therefore, the viscosity remains unchanged.
- In quadrant IV, molecules chains are oriented perpendicularly to the flow direction
  $(B_r = B_x \cos 270^o = 0)$ and again the viscosity remains unchanged.
- When the magnetic lines are parallel to the rotational axis, B_z in Fig. 5c, the molecules chains are oriented along the axis of rotation, that is, perpendicularly to the flow direction. As a result, viscosity may increase.

Lu et al. [39] measured the viscosity of the CNC aqueous suspensions on an AR–G2 rheometer (TA Instruments, USA). The measurements are taken in the shear rate ranging from 0.01 to $100\,\mathrm{s}^{-1}$. Temperature control was established with a Thermo–Cube kept within $\pm 0.05\,\mathrm{C}^o$ of the desired temperature. Shafiei et al. [40] carried out the viscosity measurements on a rotational rheometer (MCR 501 Anton Paar Physica) with parallel flat stainless steel plate geometry of $50\,\mathrm{nm}$ in diameter and $1\,\mathrm{nm}$ gap. All rheological measurements were performed at temperature of $298\,\mathrm{K}$. Then to describe the flow property, steady state shear viscosity was monitored by increasing the shear rate $\dot{\gamma}$ from 0.01 to $100\,\mathrm{s}^{-1}$.
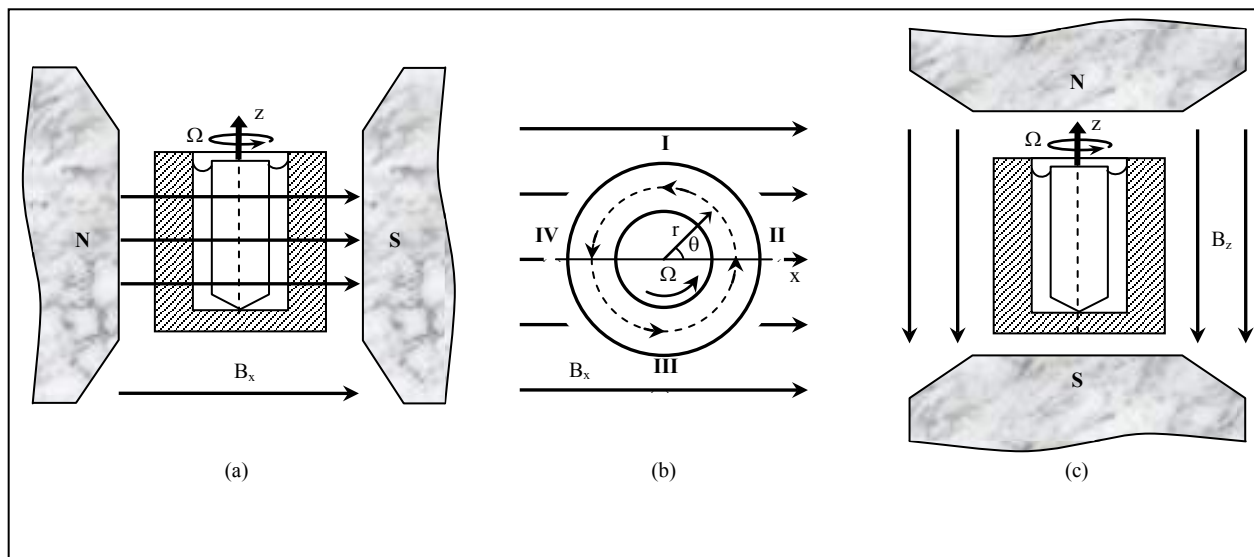
Figure 5. Schematic representation for installation method of the rheometer in magnetic field (side view), where N and S are electromagnet poles B_x and B_z are the magnetic field intensity in x– and z–directions respectively

6. Results and Discussion

6.1. Cellulose Derivatives Flow Curves

In this section fitting results of the experimental data given in [26-30] and [39, 40] are overviewed to give a coherent picture about the rheological behaviors of the considered solutions and suspensions. Four sets of cellulose derivatives experimental data were used in order to describe their rheological behavior, see Table 3. A good fit for the experimental flow curves can be obtained starting from the understanding the effects of the Giesekus parameters on the flow curve under consideration and finding the proper values for these parameters. Then by inserting the proper values in the Giesekus model explained above we can draw a theoretical curves. The proper parameters values must able the theoretical curve to catch the experimental points. Giesekus model contains four parameters: the zero shear rate viscosity (η_o), the retardation time (λ_1), the relaxation time (λ_2) and the shape factor (a). The suitable values of the four Giesekus parameters required for the best fit are listed in Table 3 for each cellulose derivative with its suitable solvents.

Figures 6 show the dependences of the viscosity of EC solutions on shear rate in the presence and in the absence of a magnetic field for 0.25wt% EC–DMAA–system (Fig. 6a), 0.3wt% EC–DMAA*–system (Fig. 6b) and 0.25wt% EC–DMF–system (Fig 6c). Similar work were obtained for other HEC, HPC and CMC solutions in Figs. 7a, 7b and 7c, Figs. 8a, 8b, 8c and Fig. 9. The studied solutions are non–Newtonian fluids, the viscosity decreases when the shear rate increases. As seen in Figs. 6 to 9, samples exhibit shear thinning over the whole shear rate range investigated. By increasing shear rate, the velocity drops significantly and its profile changes to one exhibiting three discrete regions as the following, see Fig. 6b:

- Region I in which the velocity profile consists of a shear thinning at low shear rate, a situations that indicates the breaking of the initial structures of polymer solutions.
- Region II at intermediate shear rates, where the solutions viscosity continue to decrease and the molecules chains orient along the flow direction during deformation.
- Region III at high shear rates, where the shear stress is high enough to destroy the liquid domains into individual molecule chains and orient these chains along the flow direction. Therefore, the viscosity tends to become a constant value.

To study the effects of magnetic field and shear rate on the rheological behavior of cellulose derivatives solutions, Vshivkov et al. applied two magnetic fields, one in x–direction $B_x = 3.7 \text{kOe}$ and the other in z–direction $B_z = 3.6 \text{kOe}$ to various suspensions and measured their viscosity. During analysis of the viscosity data, we must taken into account that the viscosity is affected by shear rate and the applied magnetic field. As we have seen above, the viscosity of all samples decreases with increasing shear rate and increases with increasing the applied magnetic field. Figures 6 to 9 show flow curves for all used solutions in the presence and in the absence of the magnetic field. In low concentration solutions, molecules chains are few and the field effect is insignificant. The number of molecules capable of orientation in the magnetic field increases with the polymer concentration, and the field effect on the system properties becomes stronger. The increase in solutions viscosity with concentration is related to an increasing number of magnetically sensitive molecular chains. However, at high concentrations, the number of entanglements network increases and begins to hinder the orientation processes and the influence of the field on viscosity of solutions decreases.

Table 3. Proper Parameters of Giesekus Model for Cellulose Derivatives and Their Suitable Solvents

Cellulose Derivative	Solvents	η_0 (Pa.s)			λ_1 (s)			λ_2/λ_1			a		
		B=0	B_Z=3.6	B_X=3.7	B=0	B_Z=3.6	B_X=3.7	B=0	B_Z=3.6	B_X=3.7	B=0	B_Z=3.6	B_X=3.7
EC	DMAA	76.00	118.0	113.0	0.70	0.80	0.90	0.650	0.430	0.480	0.200	0.350	0.250
	DMAA*	0.019	0.025	0.063	0.70	0.80	0.90	0.400	0.400	0.160	0.800	0.600	0.400
	DMF	88.00	112.0	127.0	0.85	1.40	1.40	0.300	0.250	0.250	0.700	0.340	0.400
HEC	DMF	1400	2000	4700	0.52	0.45	0.43	0.001	0.001	0.001	0.970	0.930	0.990
	DMF*	0.001	0.002	0.009	0.55	0.50	0.85	0.010	0.010	0.001	0.970	0.930	0.940
	Water	930.0	1100	680.0	0.95	0.95	0.93	0.051	0.010	0.010	0.250	0.700	0.990
HPC	Water	28.50	26.80	22.20	0.96	0.95	0.30	0.510	0.580	0.100	0.012	0.012	0.005
	Ethylene glycol	730.0	---	1500	0.55	---	0.55	0.130	---	0.010	0.700	---	0.800
	DMSO	1.600	2.800	3.500	0.70	0.80	0.90	0.600	0.380	0.260	0.500	0.950	0.600
	Ethanol	3.800	4.800	6.500	2.50	1.10	1.10	0.430	0.290	0.290	0.900	0.900	0.990
CMC	Water	9.100	---	12.00	1.00	---	1.20	0.001	---	0.100	0.010	---	0.010
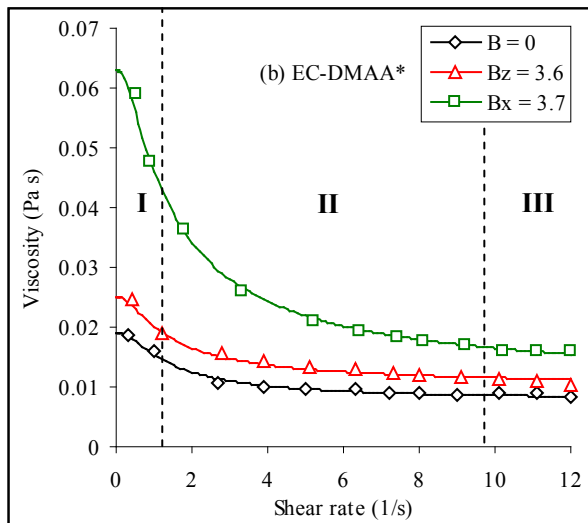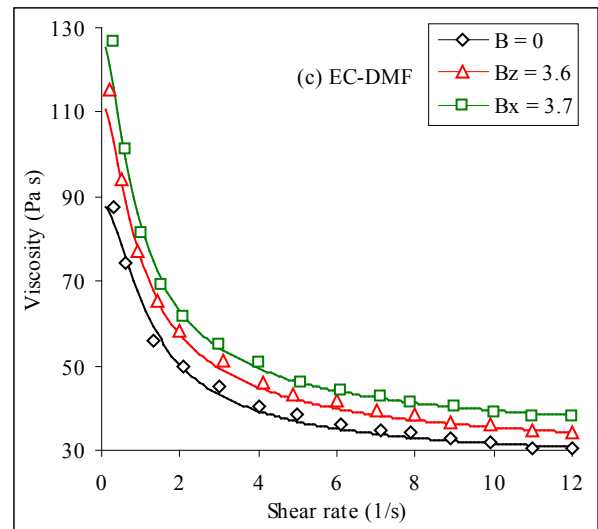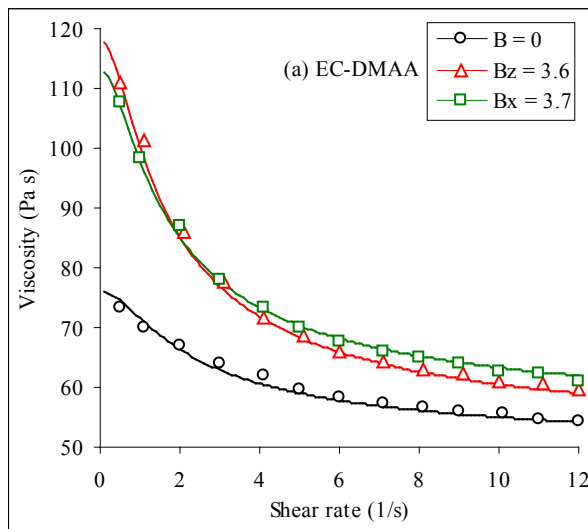
Figure 6. Viscosity–shear rate curves for EC solutions in (a) DMAA $C = 0.25\,\text{wt}\%$, (b) DMAA* $C = 0.3\,\text{wt}\%$ and (c) DMF $C = 0.25\,\text{wt}\%$ at different values of magnetic field where dots represent the experimental data taken from [26, 28, 29] and solid lines represent Giesekus model fit
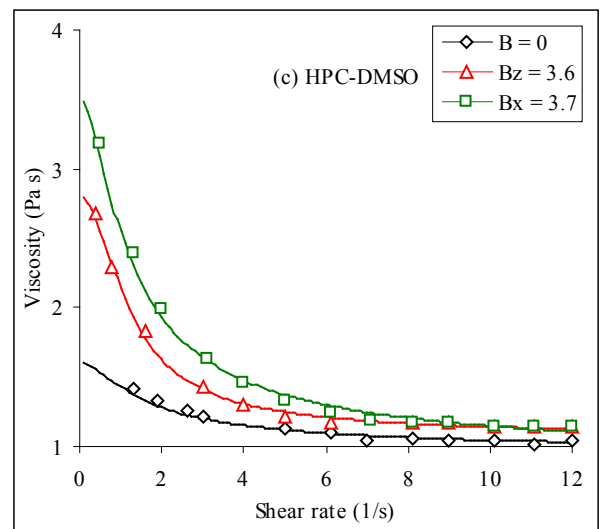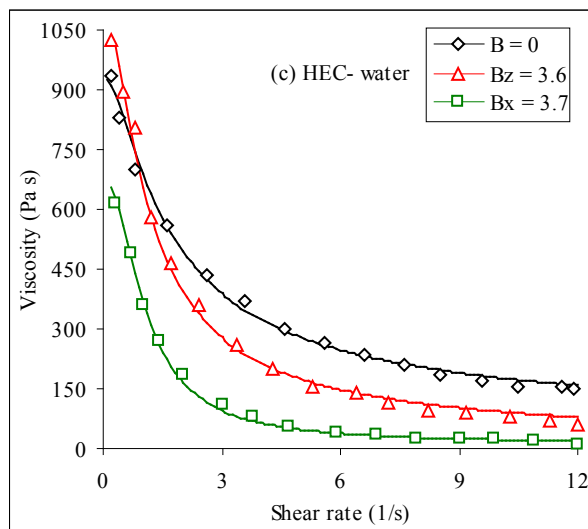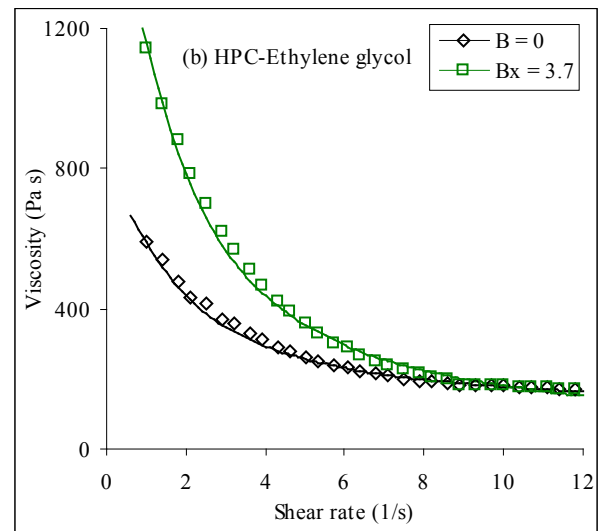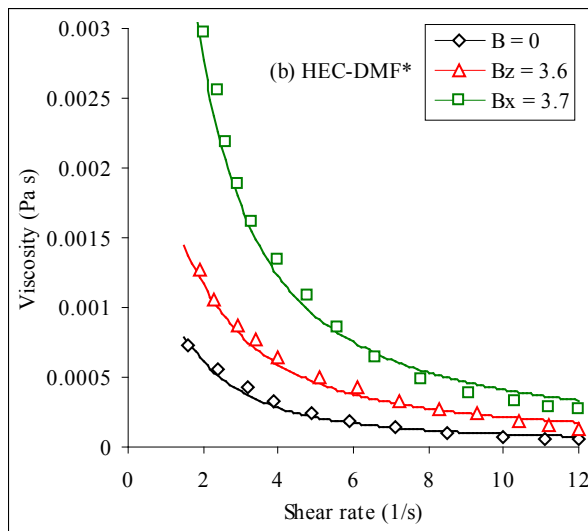
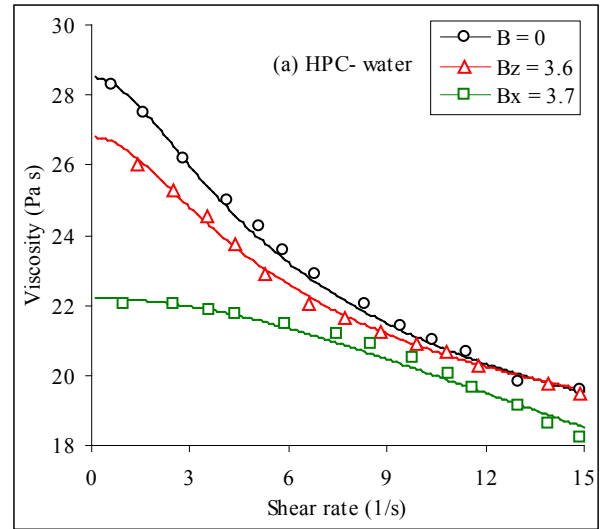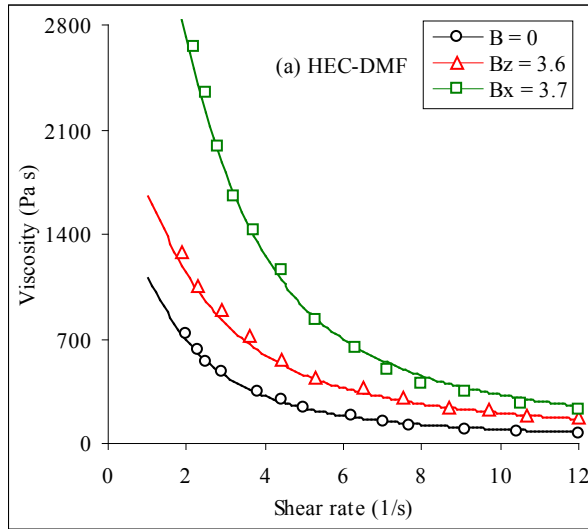**Figure 7.** Viscosity–shear rate curves for HEC solutions in (a) DMF $C = 0.15\,\text{wt\%}$, (b) DMF* $C = 0.15\,\text{wt\%}$ and (c) water $C = 0.10\,\text{wt\%}$ at different values of magnetic field where dots represent the experimental data taken from [26, 28, 26] and solid lines represent Giesekus model fit
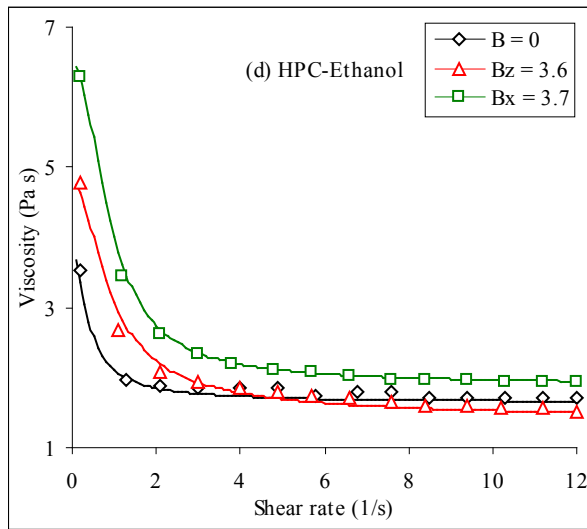
Figure 8. Viscosity–shear rate curves for HPC solutions in (a) water $C = 0.10\,\text{wt\%}$, (b) Ethylene glycol $C = 0.15\,\text{wt\%}$, (c) DMSO $C = 0.10\,\text{wt\%}$ at different values of magnetic field where dots represent the experimental data taken from [26, 29, 30] and solid lines represent Giesekus model fit

Figure 8. (d) Viscosity–shear rate curves for HPC solutions in Ethanol $C = 0.41\,wt\%$ at different values of magnetic field where dots represent the experimental data taken from [30] and solid lines represent Giesekus model fit
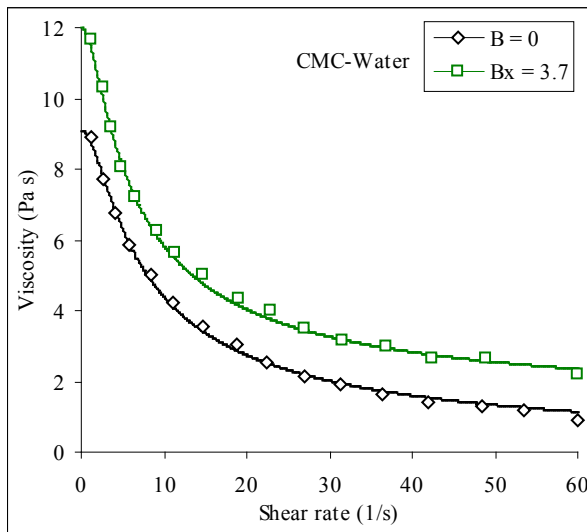

Figure 9. Viscosity–shear rate curves for CMC solutions in water $C = 0.04\,wt\%$ at different values of magnetic field where dots represent the experimental data taken from [27] and solid lines represent Giesekus model fit

6.2. Relaxation Character of Cellulose Derivatives Viscosity

To investigate the relaxation character of the viscosity behavior of cellulose derivatives solutions, Vshivkov et al. measured the solutions viscosities via two steps, shear rate was increased from 0 to $13\,s^{-1}$ for 10 min (loading) and at the second step, the shear rate was decreased from 13 to $0\,s^{-1}$ for 10 min (unloading). Figure 10a show the two successive steps of determination the viscosity values of HPC–Ethylene glycol system during loading (filled symbols) and unloading (open symbols) in the absence of the magnetic field. By

using the same sample, the loading and unloading curves do not coincide; i.e., a hysteresis loop is observed. Clearly higher viscosities for the increasing shear rate experiments are observed at low shear rates. In fact, when a test is performed the structure network of the HPC solutions is gradually destroyed as the shear rate increases. Hence, in the second experiments conducted from decreasing shear rates on the same sample, lower viscosity values are observed. From this behavior, it can be concluded that the network broken down in increasing shear test cannot be reformed with the same strength in decreasing shear test. Similar results were obtained for more concentrated HPC solutions. As shown in Fig. 10b, the application of a magnetic field results in increased viscosity values and, hence, relaxation times.
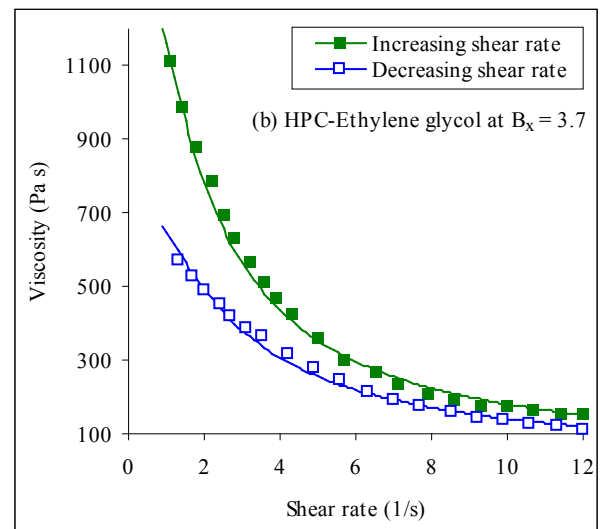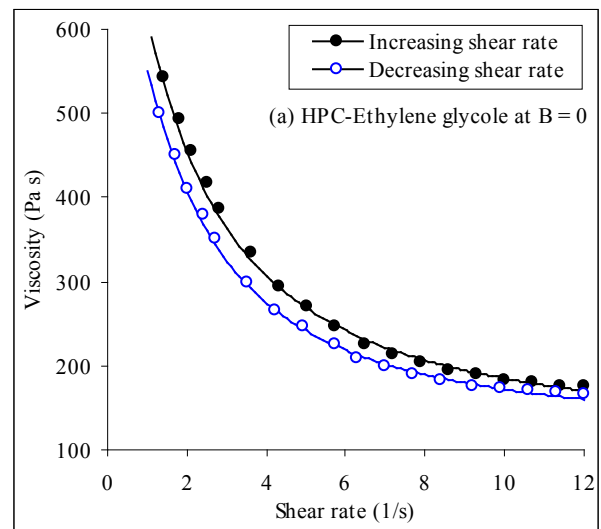

Figure 10. Viscosity–shear rate curves for HPC solution in ethylene glycol $C = 0.15\,wt\%$ for increasing and decreasing shear rate and in (a) the absence of magnetic field ($B = 0$) and (b) at $B_x = 3.7$ where dots represent the experimental data taken from [29] and solid lines represent Giesekus model fit

6.3. CNC Suspensions Flow Curves

To study the effects of shear rate on the rheological behavior of dilute aqueous CNC suspensions, data measured by Lu et al. [39] and Shafiei et al. [40] are considered. The dependence of the viscosity of CNC suspensions on shear rate as measured by Lu et al. can be seen in Fig. 11a. Data are obtained at 298K and at different values of concentrations. The range of shear rate is sufficient to cover the regions in which the viscosities at high shear rates arise to some constant values. In the range of low and intermediate shear rates, the viscosity is a function of concentration. Similar depends were obtained from that data measured by Shafiei et al. in Fig. 11b. The studied suspensions are non–Newtonian fluids, the viscosity decreases when the shear rate increases, a situations that indicates the breaking of the initial structures of polymer suspensions and the orientation of fibers along the flow direction during deformation. The velocity drops significantly and its profile changes to one exhibiting three discrete regions as the following:

- Region I in which the velocity profile consists of a shear thinning at low shear rate due to the alignment of the CNC fibers.
- Region II at intermediate shear rates, where the fibers have continuous alignment and oriented along the shear direction.
- Region III at high shear rates, where the shear stress is high enough to destroy the liquid domains into individual fibers and orient them along the flow direction.

According to Fig. 11, although the decrease in viscosity becomes level off at low concentrations, it still significant in the first shear thinning region of the viscosity profiles. The Giesekus model parameters for dilute aqueous CNC suspensions are given in Table 4.

Table 4. Giesekus Model Parameters for CNC Aqueous Suspensions at Different Concentrations

Author(s)	Concentration C wt %	Giesekus Model Parameters			
		η_o (Pa.s)	λ_1 (s)	λ_2 / λ_1	a
Lu et al. [39]	5.3	0.30	0.12	0.22	0.18
	6.6	1.12	0.15	0.10	0.24
	7.3	3.70	0.20	0.03	0.30
	8.0	7.70	0.10	0.01	0.80
Shafiei et al. [40]	0.5	2.2	3.0	0.001	0.051
	1.0	9.0	3.0	0.001	0.051
	1.5	20.0	3.0	0.008	0.051
	2.0	85.0	3.0	0.008	0.051

It is clear that, at low concentrations, the CNC suspensions behaved approximately as a Newtonian fluid i.e. η is constant for a wide range of $\dot{\gamma}$. The interaction between CNC fibers leads to increased η as the CNC concentration increased. For all samples studied by Lu et al. [39] and Shafiei et al. [40], the viscosity of these suspensions possesses viscoelastic shear thinning characteristics. This

shear thinning behavior is due to break down of NCN bond network under the application of shear and the alignment of individual CNC fibers in the direction of shear. However, it must be pointed out that the viscosity measured by Shafiei et al., Fig. 11b, at each constants shear rate and concentration are higher than those measured by Lu et al., Fig. 11a. This arises as a result of the difference in the dimensions of CNC fibers during preparation.
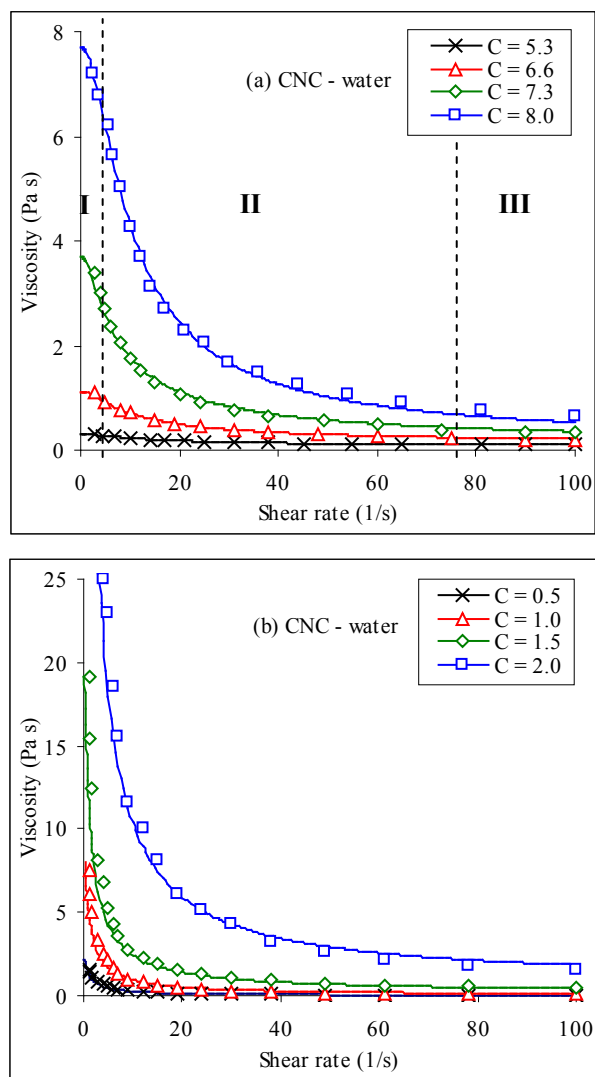

Figure 11. Viscosity–shear rate curves for CNC aqueous suspensions at different concentrations where dots represent the experimental data taken from (a) Lu et al. [39] and (b) Shafiei et al. [40] and solid lines represent Giesekus model fit

6.4. Effect of Concentration on the Viscosity of CNC Suspensions

The shear rate and viscosity properties of CNC suspensions are now well documented. They can undergo a phase shift from an isotropic to an anisotropic state before gelling. At low concentrations CNC fibers did not interact much with each other. The suspensions were characterized by a Newtonian plateau, where Brownian motion dominates over shear. As the shear increased, the hydrodynamic forces oriented particles under flow, which decreases the viscosity.

At higher concentrations, the system become biphasic with both anisotropic and isotropic phases. The relationship between the concentration of CNC suspensions and its viscosity at constant shear rates is shown in Fig.12a. It can be observed that for concentrations up to 1.5wt%, the CNC suspension presented similar behaviors, which is an increase for viscosities with the concentration. For concentration $C > 1.5wt\%$, there is a sudden increase in viscosity. We can state that the concentration functionality of CNC suspensions is due to the increase in the CNC fibers interactions. Referring to my previous paper [42] we can relate the measured viscosity to shear rate and concentration using the following formula:

$$\eta(\dot{\gamma}, C) = a_1 \, Exp(b_1 \, C) \overline{\eta}(\dot{\gamma}) , \qquad (47)$$

$$\overline{\eta} = \frac{\lambda_2}{\lambda_1} + \left(1 - \frac{\lambda_2}{\lambda_1}\right) \frac{(1-f)^2}{1+(1-2\alpha)f} , \qquad (48)$$

the function "f" in the last equation is given in Eq. (16). The values of the parameters a_1 and b_1 are calculated and a new proposed correlation which predict the viscosity of CNC suspensions is:

$$\eta(\dot{\gamma}, C) = 0.72 \, Exp(235.2\,C) \overline{\eta}(\dot{\gamma}) . \qquad (49)$$

The combined effects of shear rate and concentration on CNC suspension viscosity can be seen in Fig. 12b (in three dimensions form).

The viscosity of CNC suspensions were measured at concentrations 5.3, 6.6, 7.3, and 8wt% [39] and at 0.5, 1, 1.5, 2 and 2.5wt% [40] at $298\,K$. Figure 12 shows that, the viscosity of the suspensions with concentrations up to 1wt% showed Newtonian behaviour as the viscosities were not affected by the shear rate. However, shear thinning behaviour was observed as the viscosity decreased with increasing applied shearing stress for those concentration above 1wt%. The regions of cholesteric phase, as shown in Fig. 12a, is described by Onogi and Asada [55] for CNC suspensions. Region I corresponds to the flow of accumulate fibers. Region II corresponds to a transition state. Region III is the shear thinning of suspension of dispersed fibers under high shear forces, which spend most of their times aligned with the flow.

7. Conclusions

The objective of this work is to investigate the measured data behaviour of some cellulose derivatives (EC, HEC, HPC and CMC) dissolved in eight acceptable solvents and rheology of dilute aqueous suspensions of cellulose nanocrystals. We reconsider Vshivkov et al. measured data on Rheotest RN 4.1 rheometer for cellulose derivatives at concentrations 0.04, 0.1, 0.15, 0.25, 0.3 and 0.41wt% and Lu et al. and Shafiei et al. measured data on AR–G2 rheometer for CNC suspensions at concentrations 0.5, 1, 1.5, 2, 5.3, 6.6, 7.3 and 8 wt%. The viscosities of the analyzed solutions and suspensions were determined by fitting the data using Giesekus model for viscoelastic polymers. Advantage of using Giesekus model fit is the possibility of carrying out the theoretical analysis for viscosity measurements once an initial parameters have been performed.

As seen from the figures, all samples exhibit shear thinning over the whole shear rate range investigated. The effects of magnetic field on rheological properties of cellulose derivatives have been investigated. Polymer viscosity is decreased by increasing the magnetic field strength. This is due to the molecules of cellulose derivatives are characterized by a rigid helical configuration. These molecules orient themselves in the magnetic field so that their long chains are oriented parallel to the magnetic field lines.

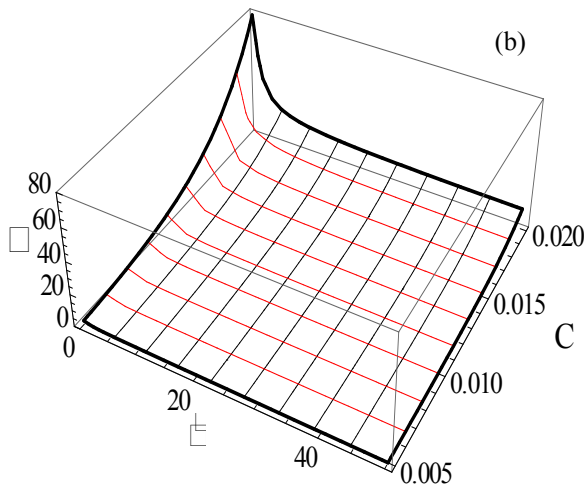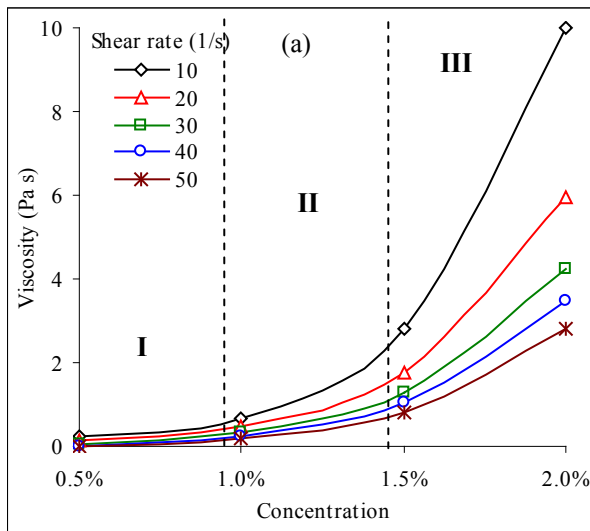The CNC suspensions exhibit a similar behavior. At low

Figure 12. (a) Concentration dependence of CNC suspension viscosity as calculated in [40] where dots represent the experimental data (b) The combined effects of $\dot{\gamma}$ and C on η of CNC suspension in 3D

where a_1 and b_1 are constants. Since Giesekus model accurately predicts the viscosity as a function of shear rate. Hence, the term $a_1 \, Exp(b_1 \, C)$ is equivalent to η_o in Eq. (13) and the term $\overline{\eta}(\dot{\gamma})$ is given by:

concentrations (up to 1wt%), the CNC suspensions have a very low viscosity almost independent of the shear rate (Newtonian behaviour) due to the Brownian motion of the CNC fibers, which prevents them to orient under flow. At very high shear rates, the shear forces tend to orient the fibers along the flow, which leads to a trivial shear thinning of the suspensions. Increasing the concentration above 1wt%, the anisotropic phase appears at low shear rates because the fibers start coming into closer contact. With the help of reported information and illustrated figures, the following conclusions can be deduced:

- The possibility of analyzing the experimental data using Giesekus model supports the fact that this model gives better and more accurate results, as it can be applied in dilute suspensions and polymeric solutions.
- Moreover, the theoretical analysis shows that cellulose derivatives solutions and CNC suspensions are characterized by five parameters (η_o, λ_1, λ_2, a and C) which must be determined when measuring the flow properties of solutions or suspensions.
- A theoretical analysis confirmed that increasing the magnetic field strength decreases the viscosity of the polymeric liquid.
- The viscosity of the solutions with low concentrations showed Newtonian behaviour as the viscosities were not affected by the shear rate. However, by increasing the concentrations the shear thinning behaviour was observed as the viscosity decreased with increased applied shearing stress.
- The drop in viscosity is very sharp as shear rate increases slightly.
- Depending on the concentration, three flow regions are observed. At low concentration, the rheological behaviour simulate a linear relationship (Newtonian fluid) which indicates that the shear rate has less effect on viscosity. While at high concentration, the shear rate has a large effect on viscosity of polymer which simulate the non–Newtonian fluids.
- Final conclusion in this paper is that, the Giesekus model able to describe the rheological properties of any viscoelastic polymer. Before embarking on this description you must first know the values of the model parameters (η_o, λ_1, λ_2, a) that make the theoretical curve catches the experimental data.

REFERENCES

[1]   S. Nishikawa, and S. Ono, Proc. Math. Phys. Soc. Tokyo, vol. 7, pp. 131, 1913.

[2]   H. Krässig, Cellulose, Polymer Monographs, vol. 11, Gordon and Breach Science Publishers, Amsterdam, 1996.

[3]   F. J. Kolpak, and J. Blackwell, "Determination of the structure of cellulose II," J. Macromolecules, vol. 9(2), pp. 273–278, 1976.

[4]   J. W. S. Hearle, "A fringed fibril theory of structure in crystalline polymers," J. Polym. Sci., vol. 28(17), pp. 432–435, March 1958.

[5]   P. J. Flory, "Statistical thermodynamics of semiflexible chain molecules," Proc. R. Soc. London, Ser. A, vol. 234, pp. 60, 1956.

[6]   R. Werbowy, and D. Gray, Macromolecules, vol. 13, pp. 69, 1980.

[7]   R. Werbowy, and D. Gray, Mol. Cryst. Liq. Cryst., vol. 34, pp. 97, 1976.

[8]   S. S. L. Tseng, A. Valente, and D. Gray, "Cholesteric liquid crystalline phases based on acetoxypropyl cellulose macromolecules," vol. 14, pp. 715–719, 1981.

[9]   A. M. Ritcey, K. R. Holme, and D. G. Gray, "Cholesteric properties of cellulose acetate and triacetate in trifluoroacetic acid," Macromolecules, vol. 21, pp. 2914–2917, 1988.

[10]   J. X. Guo, and D. Gray, "Preparation and liquid-crystalline properties of (acetyl)(ethyl) cellulose," Macromolecules, vol. 22, pp. 2082–2086, 1989.

[11]   R. Bodvik, A. Dedinaite, L. Karlson, M. Bergström, P. Bäverbäck, J. Skov Pedersen, K. Edwards, G. Karlsson, I. Varga, and P. M. Claesson, "Aggregation and network formation of aqueous methylcellulose and hydroxypropyl methylcellulose solutions," Colloids and surfaces, series A, vol. 354, pp.162–171, 2010.

[12]   H. Boerstel, H. Maatman, J. B. Westerink, and B. M. Koenders, "Liquid crystalline solutions of cellulose in phosphoric acid," Polymer, vol. 42, pp. 7371–7379, 2001.

[13]   S. A. Vshivkov, and E. V. Rusinova, "Liquid crystal phase transitions and rheological properties of cellulose ethers," Russian Journal of Applied Chemistry, vol. 84(10), pp. 1830–1835, 2011.

[14]   P. Zugenmaier, "Materials of cellulose derivatives and fiber–reinforced cellulose–polypropylene composites: characterization and application," Pure Appl. Chem., vol. 78(10), pp. 1843–1855, 2006.

[15]   P. Navard, and J. Haudin, "Rheology of mesomorphic solutions of cellulose," Br Polym. J., vol. 12(4), pp. 174–178, 1980.

[16]   T. Dahl, and A. Kibbe, Hand book of pharmaceutical excipients, American Pharmaceutical Association and Pharmaceutical Press, 2000.

[17]   M. Davidovich–Pinhas, S. Barbut, and A. G. Marangoni, "Physical structure and thermal behavior of ethyl cellulose," Cellulose, vol. 21(5), pp. 3243–3255, 2014.

[18]   C. Clasen, and W. M. Kulicke, "Determination of viscoelastic and rheo–optical material functions of water–soluble cellulose derivatives," Prog. Polym. Sci., vol. 26(9), pp. 839, 2001.

[19]   S. Y. Lin, S. L. Wang, Y. S. Wei, and M. J. Li, "Temperature effect on water desorption from methyl cellulose films studied by thermal FT–IR micro spectroscopy," Surf. Sci., vol. 601(3), pp. 781–785, 2007.

[20]   C. H. Chen, C. C. Tsai, W. Chen, F. L. Mi, H. F. Liang, S. C. Chen, and H. W. Sung, "Novel living cell sheet Harvest

system composed of thermo–reversible Methyl cellulose hydrogels," Biomacromolecules, vol. 7(3), pp. 736–743, 2006.

[21] L. Karlson, Hydrophobically modified polymers–Rheology and Molecular Associations, Lund University, Lund, 2002.

[22] T. Sanz, M. A. Fernandez, A. Salvador, J. Munoz, and S. M. Fiszman, "Thermogelation properties of methyl cellulose (MC) and their effect on a batter formula," Food Hydrocolloids, vol. 19(1), pp. 141–147, 2005.

[23] N. Gowariker, Viswanathan, and J. Sreedhar, Polymer Science, John Wiley and Sons, 1986.

[24] D. Gray, and H. Darley, Composition and properties of oil well drilling fluids, 4th ed., Gulf Publication Co., Houston, 1981.

[25] S. A. Vshivkov, Phase transitions of polymer systems in external fields, Lan. Sankt–Peterburg, 2013.

[26] S. A. Vshivkov, E. V. Rusinova, and A. G. Galyas, "Phase diagrams and rheological properties of cellulose ether solutions in magnetic field," Eur. Polym. J., vol. 59, pp. 326–332, 2014.

[27] S. A. Vshivkov, and A. A. Byzov, "Phase equilibrium, structure, and rheological properties of the carboxymethyl cellulose–water system," Polym. Sci., Ser. A, vol. 55(2), pp. 102–106, 2013.

[28] S. A. Vshivkov, E. V. Rusinova, and A. G. Galyas, "Effect of a magnetic field on the rheological properties of cellulose ether solutions," Polym. Sci A, vol. 54(11), pp. 827–832, 2012.

[29] S. A. Vshivkov, and T. S. Soliman, "Phase Transitions, structures, and rheological properties of hydroxypropyl cellulose–ethylene glycol and ethyl cellulose–dimethyl formamide systems in the presence and in the absence of a magnetic field," Polym. Sci., series A, vol. 58(4), pp. 499–505, 2016.

[30] S. A. Vshivkov, and T. S. Soliman, "Effect of a magnetic field on the rheological properties of the systems hydroxypropyl cellulose-ethanol and hydroxypropyl cellulose-dimethylsulfoxide," Polym. Sci., series A, vol. 58(3), pp. 307–314, 2016.

[31] X. M. Dong, T. Kimura, J. F. Revol, and D. G. Gray, "Effects of ionic strength on the isotropic–chiral nematic phase transition of suspensions of cellulose crystallites," Langmuir, vol. 12(8), pp. 2076–2082, 1996.

[32] Y. Habibi, L. A. Lucia, and O. J. Rojas, "Cellulose nanocrystals: chemistry, self–assembly, and applications," Chem. Rev., vol. 110(6), pp.3479–3500, 2010.

[33] R. J. Moon, A. Martini, J. Nairn, J. Simonsen, and J. Youngblood, "Cellulose nanomaterials review: structure, properties and nanocomposites," Chem. Soc. Rev., vol. 40(7), pp. 3941–3994, 2011.

[34] M. Bercea, and P. Navard, "Shear dynamics of aqueous suspensions of cellulose whiskers," Macromolecules, vol. 33(16), pp. 6011–6016, 2000.

[35] E. Lasseuguette, D. Roux, and Y. Nishiyama, "Rheological properties of microfibrillar suspension of TEMPO–oxidized pulp," Cellulose, vol. 15(3), pp. 425–433, 2008.

[36] G. Agoda–Tandjawa, S. Durand, S. Berot, C. Blassel, C. Gaillard, C. Garnier, and J. L. Doublier, "Rheological characterization of microfibrillated cellulose suspensions after freezing," Carbohydr Polym., vol. 80(3), pp. 677–686, (2010).

[37] M. Bercea, and P. Navard, "Shear dynamics of aqueous suspensions of cellulose whiskers," Macromolecules, vol. 33(16), pp. 6011–6016, 2000.

[38] E. E. Urena–Benavides, G. Ao, V. A. Davis, and C. L. Kitchens, "Rheology and phase behavior of lyotropic cellulose nanocrystal suspensions," Macromolecules, vol. 44(22), pp. 8990–8998, 2011.

[39] A. Lu, U. Hemraz, Z. Khalili and Y. Boluk, "Unique viscoelastic behaviors of colloidal nanocrystalline cellulose aqueous suspensions," Cellulose, vol. 21, pp. 1239–1250, 2014.

[40] S. Shafiei–Sabet, M. Martinez, and J. Olson, "Shear rheology of micro–fibrillar cellulose aqueous suspensions," Cellulose, vol. 23, pp. 2943–2953, 2016.

[41] S. E. E. Hamza, "A comparison of rheological models and experimental data of Metallocene linear low density Polyethylene solutions as a function of temperature and concentration," Journal of advances in physics, vol. 12(3), pp. 4322–4339, 2016.

[42] S. E. E. Hamza, "Modelling the effect of concentration on non–Newtonian apparent viscosity of an aqueous Polyacrylamide solution," Global Journal of Physics, vol. 5(1), pp. 505–517, 2016.

[43] S. G. Advani, and C. L. Tucker, "Closure approximations for three dimensional structure tensors," J. Rheol., vol. 34(3). pp 367–386, 1990.

[44] H. Giesekus, "Stressing behavior in simple shear flow as predicted by a new constitutive model for polymer fluids," J. Non–Newtonian Fluid Mech., vol. 12, pp. 367–374, 1983.

[45] H. Giesekus, "A simple constitutive equation for polymer fluids based on the concept of deformation dependent tensorial mobility," J. Non–Newtonian Fluid Mech., vol. 11, pp. 69–109, 1982.

[46] R. B. Bird, C. F. Curtiss, R. C. Armstrong, and O. Hassager, Dynamics of Polymeric Liquids, 2nd ed., vol. 2, Kinetic Theory, Wiley Interscience, New York, 1987.

[47] V. N. Kalashnikov, "Shear rate dependent viscosity of dilute polymer solutions," J. Rheol., vol. 38(5), pp. 1385–1403, 1994.

[48] W. Pabst, "Fundamental considerations on suspension rheology," Ceramics Silikaty, vol. 48(1), pp. 6–13, 2004.

[49] F. Rodriguez, Principles of polymer systems, 2nd ed., McGraw Hill chemical engineering series, 1983.

[50] G. L. Hand, "A theory of dilute suspensions," Arch. Ration. Mech. Anal., vol. 7, pp. 81–86, 1961.

[51] C. Crowe, "Review numerical models for dilute gas particles flow," J. Fluids Eng., Tran. ASME, vol. 104, pp. 297–303, 1982.

[52] S. G. Advani, and E. M. Sozer, Process modeling in composites manufacturing, Marcel Dekker Inc., New York, 2003.

[53] G. L. Hand, "A theory of anisotropic fluids," J. Fluid Mech., vol. 13, pp. 33–62, 1962.

[54] S. E. E. Hamza, "Basic concepts of rigid fiber suspensions rheology," Global Journal of Physics, vol. 5(2), pp. 562–584, 2017.

[55] S. Onogi, and T. Asada, "Rheology and rheo–optics of polymer liquid crystals," Rheology, vol. 1, pp 127–147, 1980.